



Aerosol assisted chemical vapour deposition of transparent conductive aluminum-doped zinc oxide thin films from a zinc triflate precursor

Joe A. ManziDr., Caroline E. KnappDr., Ivan P. ParkinProf., Claire J. CarmaltProf. *

Materials Chemistry Centre, Department of Chemistry, University College London, 20 Gordon Street, London WC1H 0AJ, UK

ARTICLE INFO

Article history:

Received 10 May 2016

Received in revised form 23 August 2016

Accepted 4 September 2016

Available online 06 September 2016

Keywords:

Zinc oxide

Zinc triflate

Transparent conducting oxide

Thin films

Aerosol assisted chemical vapour deposition

ABSTRACT

The use of zinc triflate (trifluoromethanesulfonate), $[\text{Zn}(\text{OTf})_2]$ as a precursor in the aerosol assisted chemical vapour deposition of zinc oxide thin films is described. Aluminum doped zinc oxide (AZO) thin films are also shown to be deposited when aluminum acetylacetonate $[\text{Al}(\text{acac})_3]$ was introduced into the precursor solution, illustrating the versatility of this system. Film characterization techniques include glancing angle X-ray powder diffraction, X-ray photoelectron spectroscopy, scanning electron microscopy and optical and electrical measurements. AZO films with an Al content of 7 at.% were found to have favourable transparent conducting oxide properties with simultaneous high transparency ($>80\%$) in the visible light region and a low electrical resistivity ($1.96 \times 10^{-3} \Omega \text{ cm}$).

© 2016 Elsevier B.V. All rights reserved.

1. Introduction

Zinc oxide (ZnO) is a II–VI semiconductor material and one of only a few materials that can combine high optical transparency with low electrical resistivity to act as a transparent conducting oxide (TCO) material. Thin films of nominally undoped ZnO exhibit *n*-type conductivity, traditionally attributed to native point defects such as zinc interstitials or oxygen vacancies. However, computational studies suggest the unintentional incorporation of hydrogen contributes significantly to the observed conductivity [1]. The conductivity can be increased upon doping with an extrinsic dopant source, such as Al or Ga, creating shallow donor states close to the conduction band of ZnO. At present, the leading commercial TCO material is indium tin oxide (ITO) [2] which is used in a number of applications such as the transparent electrode in flat panel displays, or in solar cells and organic light emitting diodes [3,4]. Alternative TCO materials are sought to replace ITO, driven in part by the high and volatile cost of indium and its short supply, reflected in the price of ITO and the subsequent electronic devices in which ITO is used [5]. TCO materials of doped ZnO and SnO_2 address these issues relating to the use of ITO whilst also exhibiting the potential to meet the demands for ever improved film properties from the commercial technology sector [6]. Aluminum doped ZnO (AZO) is a particularly promising candidate due to its ITO comparable TCO properties and the non-toxicity, abundance and relative inexpensive use of Zn [7].

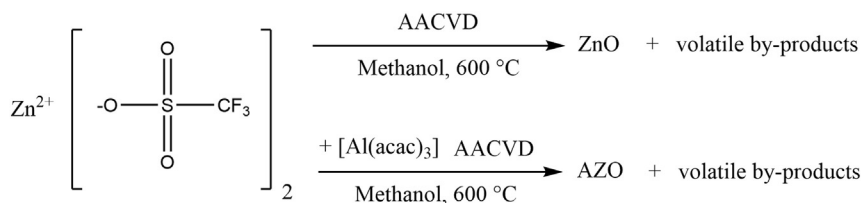
ZnO and AZO have been deposited by a number of routes including physical vapour deposition methods such as pulsed laser deposition

(PLD) [8] and sputtering [9] and by solution based methods such as spray pyrolysis [10] and sol–gel [11]. Chemical vapour deposition (CVD) is also widely used in variations including metal organic (MO)CVD [12], low pressure (LP)CVD [13], plasma enhanced (PE)CVD [14] and aerosol-assisted (AA)CVD [15,16]. AACVD has a number of advantages that have been discussed in detail by Hou and Choy [17] and more recently by Carmalt and co-workers [18,19]. Since the precursor is dissolved in a suitable solvent and delivered in the form of aerosol droplets, the requirement that a precursor be volatile is removed allowing for a greater selection of potential precursor compounds [20,21].

The most widely used zinc precursor for CVD is diethylzinc [22], however, its pyrophoric nature and high reactivity [23] make it difficult to handle and can lead to undesired and problematic pre-reaction and deposition issues. These issues drive research into other precursor systems including synthesised compounds, such as alkyl zinc alkoxides [24] and zinc β -iminoesters [25]. Other commercially available compounds including zinc acetate [26] and zinc acetylacetonate [27] have been investigated, but their use has been limited by unfavourable thermal properties [28]. One relatively inexpensive, air stable and commercially available zinc complex which has not been used as a CVD precursor, is zinc triflate $[\text{Zn}(\text{OTf})_2]$ ($\text{OTf} = \text{CF}_3\text{SO}_3$). Used in organic chemistry as a catalyst for a variety of reactions [29,30], zinc triflate has also been used in inorganic chemistry by Granum et al. [31] as a starting material for the synthesis of zinc β -ketoiminate complexes. Using AACVD to overcome its lack of volatility, we report the first use of zinc triflate as a zinc precursor in the AACVD of ZnO thin films. The potential of this facile route is exemplified in the synthesis of AZO thin films when aluminum acetylacetonate $[\text{Al}(\text{acac})_3]$ is added as a dopant source with the zinc triflate.

* Corresponding author.

E-mail address: c.j.carmalt@ucl.ac.uk (C.J. Carmalt).



Scheme 1. AACVD of ZnO and AZO thin films from $[\text{Zn}(\text{OTf})_2]$ and $[\text{Al}(\text{acac})_3]$ precursors.

2. Experimental section

2.1. General procedures

Nitrogen (99.99%) was obtained from BOC and used as supplied. Zinc triflate was procured from Sigma-Aldrich and aluminum acetylacetonate from Merck Millipore, both used as supplied. Methanol was dried over magnesium methoxide and distilled under nitrogen. ZnO thin films were deposited from a precursor solution of $[\text{Zn}(\text{OTf})_2]$ (0.5 g, 1.38 mmol) dissolved in dry methanol (30 mL). Aluminum doping was achieved by the addition of $[\text{Al}(\text{acac})_3]$ (0.022 g, 0.069 mmol) to $[\text{Zn}(\text{OTf})_2]$ (0.5 g, 1.38 mmol) in methanol (30 mL). Precursor solutions were formed in an AACVD glass bubbler flask which has an inlet valve for the carrier gas and an outlet valve for the aerosol. After 10 min of stirring, a Liquifog® piezo ultrasonic atomizer was used to create an aerosol from the precursor solution which was carried in an N_2 carrier gas out of the bubbler through a brass baffle into the cold-walled, horizontal-bed CVD reactor. The reactor was fitted with a graphite block containing a Whatman cartridge heater, used to heat the glass substrate, the temperature of which was controlled and monitored using a Platinum-Rhodium thermocouple. Films were deposited onto Pilkington NSG float glass substrates (145 mm \times 45 mm \times 4 mm) with a 25 nm barrier layer of crystalline SiO_2 . A second glass plate was held 6 mm above the glass substrate in order to quash any air turbulence and ensure a laminar gas flow. Prior to deposition the glass substrate was cleaned using isopropyl alcohol and acetone. Depositions were carried out at a substrate temperature of 600 $^\circ\text{C}$. The temperature was limited in range by the decomposition temperature of the zinc triflate precursor of 520–565 $^\circ\text{C}$ (see precursor studies) and the melting temperature of the underlying glass substrate. A flow rate of N_2 of 1.2 L min^{-1} was found to give the best substrate coverage and deposition times varied between 30 and 35 min. After deposition, the glass substrates were allowed to cool under a flow of nitrogen to below 100 $^\circ\text{C}$ before being removed.

2.2. Film analysis methods

Thermal gravimetric analysis (TGA) and differential scanning calorimetry (DSC) were carried out from room temperature (23 $^\circ\text{C}$) to 600 $^\circ\text{C}$ under helium in open aluminum pans using a Netzsch STA 449 C Jupiter Thermo-microbalance. X-ray diffraction (XRD) patterns were recorded on a Bruker D8 Discover X-ray diffractometer using monochromatic $\text{Cu } K_{\alpha 1}$ and $\text{Cu } K_{\alpha 2}$ radiation of wavelengths 1.54056 and 1.54439 Å respectively, emitted with a voltage of 40 kV and a current of 40 mA. Scanning electron microscopy (SEM) was performed using a Philips XL30 FEG operating in plane and cross section mode at varying instrument magnifications from $\times 10,000$ to $\times 50,000$. Film thickness was estimated using a Filmetrics F20 thin film measurement system. X-ray photoelectron spectroscopy (XPS) surface and depth profiling was performed using a Thermo Scientific K-Alpha XPS system using monochromatic $\text{Al } K_{\alpha}$ radiation at 1486.6 eV X-ray source. Etching was achieved using an Ar ion etch beam at 1 keV with a current of 1.55 μA . 180 levels of 30 second etching were performed. The spectral regions for Zn 2p, O 1s, Al 2p and C 1s were scanned as well as a survey spectrum to detect any additional elements. CasaXPS software was used to analyse the data with binding energies referenced to an adventitious

C 1s peak at 284.8 eV. UV/Vis/NIR transmission spectra were recorded using a PerkinElmer Lambda 950 spectrometer in the range of 250–1400 nm, following an air background correction. Sheet resistance measurements were recorded using the Van der Pauw method and Hall Effect measurements made to determine the mobility and free carrier concentrations of the deposited films.

3. Results and discussion

ZnO thin films were deposited from the AACVD of $[\text{Zn}(\text{OTf})_2]$ in methanol at 600 $^\circ\text{C}$ on SiO_2 coated float glass substrates (Scheme 1). The addition of $[\text{Al}(\text{acac})_3]$ (between 0.02 and 0.2 Al:Zn molar ratio) resulted in the deposition of AZO films (Scheme 1), where the best functional properties (transparency/conductivity) were observed when Al was added in a Al:Zn molar ratio of 0.05:1. The aluminum doping of these films was found to be 7 at.% (XPS).

The films exhibited good uniformity and coverage with deposition observed to occur on both the glass substrate and top plate as a result of thermophoretic effects [32]. Films exhibited strong adherence to the glass substrate, passing the Scotch® tape test and only being removed upon intense scratching with a steel scalpel. Solubility testing indicated that the films were insoluble in common solvents (ethanol, THF, toluene and 2-propanol) but were removed in nitric acid (2 M). Deposited films also appeared highly transparent with only a very light brown tint, indicative of low level carbon contamination.

3.1. Precursor studies

TGA and DSC (Fig. 1) were performed on the $[\text{Zn}(\text{OTf})_2]$ precursor between room temperature and 600 $^\circ\text{C}$ under helium. The initial mass loss observed in the TGA profile occurred between 40 and 120 $^\circ\text{C}$ and represented a 7–8% reduction in mass. Since $[\text{Zn}(\text{OTf})_2]$ is a hygroscopic powder, this mass loss is likely to be the loss of a residual solvent and water.

The mass was stable until the onset of the decomposition at 500 $^\circ\text{C}$ in which a clean, single step decomposition predominantly between 520

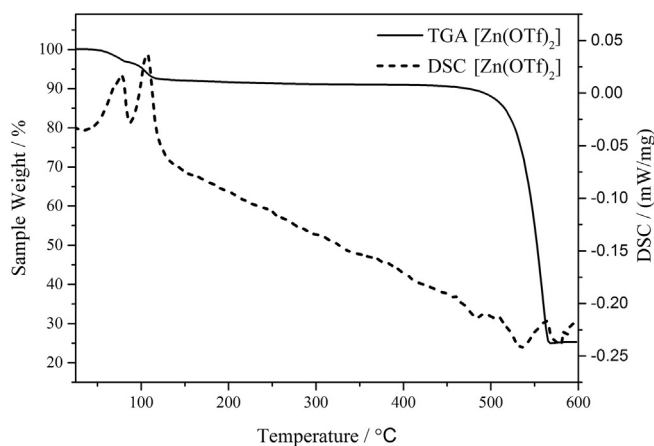


Fig. 1. Thermal gravimetric analysis (TGA) and differential scanning calorimetry (DSC) of $[\text{Zn}(\text{OTf})_2]$.

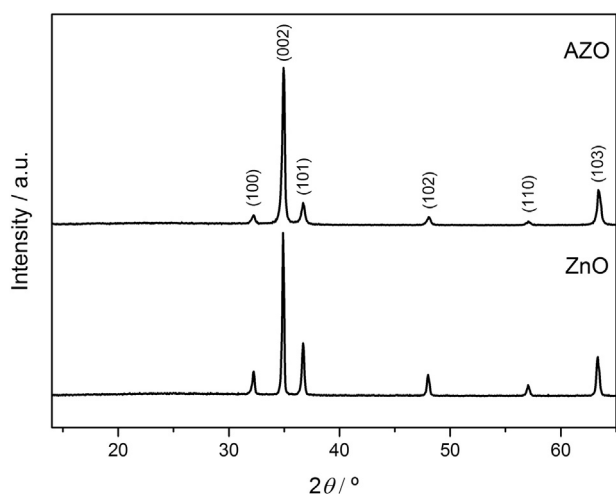


Fig. 2. XRD pattern of the ZnO and AZO thin films.

and 565 °C was observed. The residual mass (accounting for the initial mass loss) was 22.7%, which compares closely to the calculated residual mass for ZnO from $[\text{Zn}(\text{OTf})_2]$ of 22.4%. The indication of decomposition to ZnO and the clean one step decomposition profile are desired precursor properties.

3.2. X-ray diffraction

Glancing angle X-ray diffraction (XRD) patterns of the films were recorded (Fig. 2) and as expected, confirmed the formation of hexagonal wurtzite ZnO. Significant preferred orientation was observed along the (002) plane resulting from the packing of the crystallites occurring along the *c*-axis, perpendicular to the underlying substrate.

The same crystal structure was also observed for the AZO film but with a small decrease in the calculated lattice parameters, where $a = 3.25261(25)$ Å and $c = 5.20693(19)$ Å, compared to $a = 3.25428(14)$ Å and $c = 5.20975(16)$ Å for the ZnO thin film. This small decrease is indicative of Al doping into the ZnO matrix and results from the difference in ionic radius between the Zn^{2+} and Al^{3+} ions of 0.72 and 0.53 Å respectively [33]. The respective peaks in the AZO pattern are also broader, most likely resulting from the strain introduced from the Al doping.

3.3. Scanning electron microscopy

Scanning electron microscopy (SEM) images (Fig. 3A–F) show a film structure of rounded agglomerated particles, indicative of a Volmer–Weber type island growth mechanism. The surface morphology of the ZnO films appears not to change upon doping with Al and the plane view image of the AZO film at $\times 50,000$ magnification (Fig. 3C) illustrates in greater detail the particle cluster growth of the film.

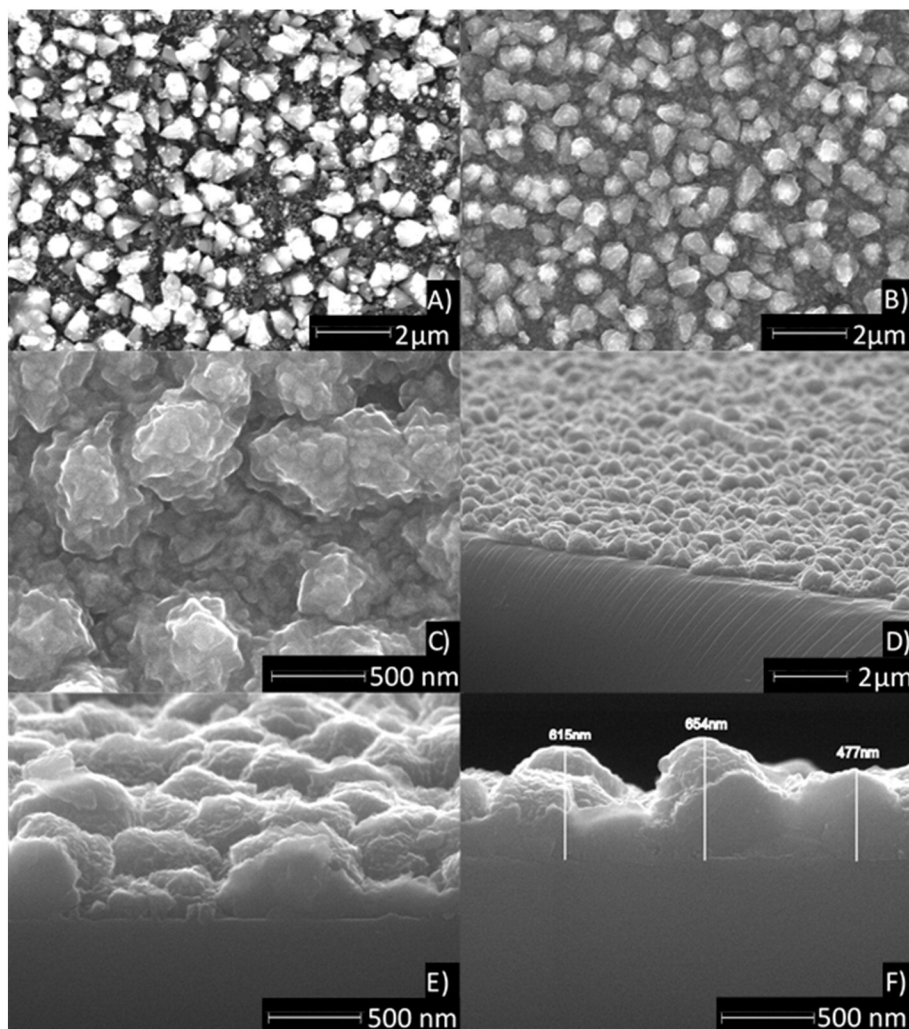


Fig. 3. SEM images of A) ZnO and B)–F) AZO films. Images in A)–C) plane view and D)–F) cross sectional view.

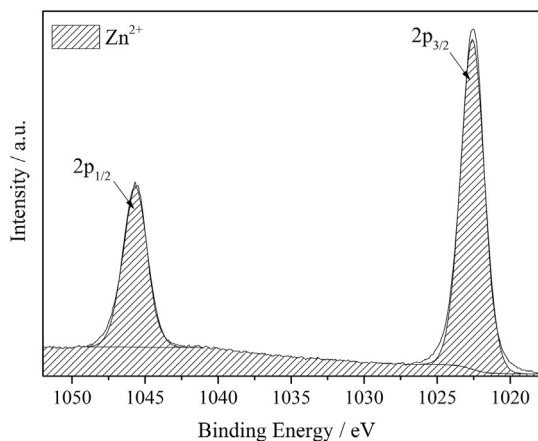


Fig. 4. XPS of Zn 2p for the AZO film.

Cross sectional images (Fig. 3D–E) show the coatings consisted of larger agglomerates of particles and smaller groupings of particles between them, resulting in rough films with noticeable height differences (Fig. 3F). The lowest thickness of film was 250 nm with the highest cluster point being 655 nm. Average film thickness was also measured using a Filmetrics analyzer system and for the AZO films a thickness range of 470–500 nm was recorded.

3.4. X-ray photoelectron spectroscopy

XPS of the ZnO and AZO films deposited from $[\text{Zn}(\text{OTf})_2]$ at 600 °C confirmed the presence of Zn and O and were consistent with XRD that solely ZnO had been deposited. Peaks were observed for the Zn $2p_{1/2}$ and $2p_{3/2}$ states at 1045.3 and 1022.2 eV binding energy respectively, as expected, with an intensity ratio of 1:2 and an energy gap of 23.1 eV (Fig. 4) [34].

The depth profile for the AZO thin film deposited from a precursor solution of Al:Zn in a molar ratio of 0.05:1 (Fig. 5) revealed the sample to be predominantly ZnO with an average Al concentration of 7 at.%. Although high levels of carbon contamination were detected at the surface it decreased to low levels in the bulk of the film.

3.5. Optical properties

The transmission characteristics of the ZnO and AZO films were investigated using UV/vis/near IR spectrometry, recorded between 250

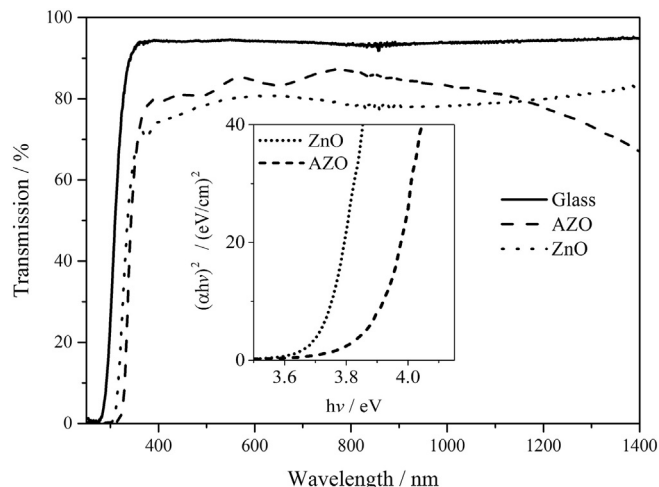


Fig. 6. Transmission spectrum for ZnO and AZO films, inset: Tauc plots for the ZnO and AZO films.

and 1400 nm (Fig. 6). The ZnO and AZO films have an average transparency of 79% (peaking at 80%) and 83% (peaking at 85%) respectively, comparing well to the >80%, a value often quoted for films described as highly transparent [35].

The sharp decrease in transmission of the deposited films between 300 and 400 nm is a result of the onset of fundamental adsorption. This has been used to estimate the optical band gap of the films using the Tauc relation [36] by finding the intercept of the $h\nu$ axis from a line of steepest gradient for the linear region of a $(\alpha h\nu)^{1/2}$ vs. $h\nu$ plot (Fig. 6 (inset)). The band gap of the ZnO and AZO films were determined to be 3.7 and 3.9 eV respectively. The band gap of the ZnO film is higher than that of bulk ZnO (3.3 eV) [37], which has previously been observed for other ZnO thin films [38,39]. The increase in band gap between the ZnO and AZO films is indicative of Al doping and results from the Burstein-Moss effect [40,41] in which the additional electrons populate the lower levels of the conduction band.

3.6. Electrical properties

Four-point probe measurements were taken of the ZnO and AZO films deposited at 600 °C. The films were conductive with sheet resistances of 70 Ω/\square for ZnO, decreasing to 15 Ω/\square for the AZO film. This value is comparable with other reported literature values for AZO deposited by AACVD where a minimum sheet resistance of 18 Ω/\square was achieved with a 6 at.% doping of Al [42]. The ZnO films had a carrier concentration of $2.24 \times 10^{20} \text{ cm}^{-3}$, mobility value of $9.3 \text{ cm}^2 (\text{V s})^{-1}$ and resistivity of $2.86 \times 10^{-3} \Omega \text{ cm}$. The doped AZO films had an increased carrier concentration and mobility of $3.03 \times 10^{20} \text{ cm}^{-3}$ and $10.5 \text{ cm}^2 (\text{V s})^{-1}$ respectively resulting in a decrease in the observed resistivity to $1.96 \times 10^{-3} \Omega \text{ cm}$. However, further investigations are required as more expensive deposition techniques, such as rf magnetron sputtering, have produced AZO films with a sheet resistance as low as 4.9 Ω/\square for films with 78% optical transparency and 10.9 Ω/\square for films with 83% optical transparency [43].

4. Conclusion

This paper reports the first deposition of ZnO from $[\text{Zn}(\text{OTf})_2]$ via AACVD. TGA and DSC analysis of $[\text{Zn}(\text{OTf})_2]$ showed the precursor to have good thermal properties and ZnO films with a transparency of 79% and a low sheet resistance of 70 Ω/\square were deposited. When $[\text{Al}(\text{acac})_3]$ was added to the precursor solution at a molar ratio of Al:Zn ratio of 0.05:1, AZO films were deposited. Optimal coverage and adherence observed using a deposition temperature of 600 °C resulting in films with the crystalline hexagonal wurtzite crystal structure of ZnO

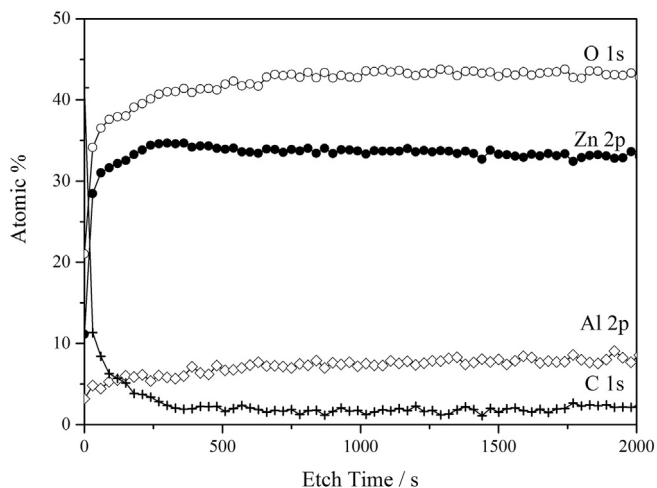


Fig. 5. XPS depth profile for the AZO thin film.

with significant preferred orientation was observed along the (002) plane. An AZO thin film with 7 at.% Al with promising TCO properties (average transparency of 83% and a low sheet resistance of $15 \Omega/\square$) was deposited.

Acknowledgements

The Engineering and Physical Sciences Research Council (EPSRC) is thanked for studentship funding (J. A. M.) through the Molecular Modelling and Materials Science Doctoral Training Centre (EP/G036675) and the grants EP/K001515 and EP/L017709. NSG Pilkington are thanked for SEM and XPS analysis and funding (J. A. M.). Deborah Raisbeck (NSG Pilkington) is thanked for assistance provided.

References

- [1] C.G. Van de Walle, Hydrogen as a cause of doping in zinc oxide, *Phys. Rev. Lett.* 85 (2000) 1012–1015, <http://dx.doi.org/10.1103/PhysRevLett.85.1012>.
- [2] C.G. Granqvist, Transparent conductors as solar energy materials: a panoramic review, *Sol. Energy Mater. Sol. Cells* 91 (2007) 1529–1598, <http://dx.doi.org/10.1016/j.solmat.2007.04.031>.
- [3] U. Betz, M. Kharrazi Olsson, J. Marthy, M.F. Escolá, F. Atamny, Thin films engineering of indium tin oxide: large area flat panel displays application, *Surf. Coat. Technol.* 200 (2006) 5751–5759, <http://dx.doi.org/10.1016/j.surfcoat.2005.08.144>.
- [4] Y.-H. Tak, K.-B. Kim, H.-G. Park, K.-H. Lee, J.-R. Lee, Criteria for ITO (indium–tin–oxide) thin film as the bottom electrode of an organic light emitting diode, *Thin Solid Films* 411 (2002) 12–16, [http://dx.doi.org/10.1016/S0040-6090\(02\)00165-7](http://dx.doi.org/10.1016/S0040-6090(02)00165-7).
- [5] D.S. Hecht, L. Hu, G. Irvin, Emerging transparent electrodes based on thin films of carbon nanotubes, graphene, and metallic nanostructures, *Adv. Mater.* 23 (2011) 1482–1513, <http://dx.doi.org/10.1002/adma.201003188>.
- [6] N. Noor, I.P. Parkin, Enhanced transparent-conducting fluorine-doped tin oxide films formed by Aerosol-assisted Chemical Vapour Deposition, *J. Mater. Chem. C* 1 (2013) 984–996, <http://dx.doi.org/10.1039/C2TC00400C>.
- [7] T. Minami, Transparent conducting oxide semiconductors for transparent electrodes, *Semicond. Sci. Technol.* 20 (2005) S35–S44, <http://dx.doi.org/10.1088/0268-1242/20/4/004>.
- [8] M.A. Bodea, G. Sbarcea, G.V. Naik, A. Boltasheva, T.A. Klar, J.D. Pedarnig, Negative permittivity of ZnO thin films prepared from aluminum and gallium doped ceramics via pulsed-laser deposition, *Appl. Phys. A Mater. Sci. Process.* 110 (2013) 929–934, <http://dx.doi.org/10.1007/s00339-012-7198-6>.
- [9] A. Mosbah, M.S. Aida, Influence of deposition temperature on structural, optical and electrical properties of sputtered Al doped ZnO thin films, *J. Alloys Compd.* 515 (2012) 149–153, <http://dx.doi.org/10.1016/j.jallcom.2011.11.113>.
- [10] E. Arca, K. Fleischer, I.V. Shvets, Influence of the precursors and chemical composition of the solution on the properties of ZnO thin films grown by spray pyrolysis, *J. Phys. Chem. C* 113 (2009) 21074–21081, <http://dx.doi.org/10.1021/jp907990z>.
- [11] J. Zhang, W. Que, Preparation and characterization of sol–gel Al-doped ZnO thin films and ZnO nanowire arrays grown on Al-doped ZnO seed layer by hydrothermal method, *Sol. Energy Mater. Sol. Cells* 94 (2010) 2181–2186, <http://dx.doi.org/10.1016/j.solmat.2010.07.009>.
- [12] J. Su, C. Tang, Q. Niu, C. Zang, Y. Zhang, Z. Fu, Microstructure, optical and electrical properties of Al-doped ZnO films grown by MOCVD, *Appl. Surf. Sci.* 258 (2012) 8595–8598, <http://dx.doi.org/10.1016/j.apsusc.2012.05.056>.
- [13] A.L. Johnson, N. Hollingsworth, G. Kociok-Köhn, K.C. Molloy, Organozinc aminoalcohols: synthesis, structure, and materials chemistry, *Inorg. Chem.* 47 (2008) 12040–12048, <http://dx.doi.org/10.1021/ic801591d>.
- [14] I. Volintiru, M. Creatore, B.J. Kniknie, C.I.M.A. Spee, M.C.M. van de Sanden, Evolution of the electrical and structural properties during the growth of Al doped ZnO films by remote plasma-enhanced metalorganic chemical vapor deposition, *J. Appl. Phys.* 102 (2007) 43709, <http://dx.doi.org/10.1063/1.2772569>.
- [15] M.R. Waugh, G. Hyett, I.P. Parkin, Zinc oxide thin films grown by aerosol assisted CVD, *Chem. Vap. Depos.* 14 (2008) 366–372, <http://dx.doi.org/10.1002/cvde.200806718>.
- [16] G. Walters, I.P. Parkin, Aerosol assisted chemical vapour deposition of ZnO films on glass with noble metal and p-type dopants; use of dopants to influence preferred orientation, *Appl. Surf. Sci.* 255 (2009) 6555–6560, <http://dx.doi.org/10.1016/j.apsusc.2009.02.039>.
- [17] X. Hou, K.-L. Choy, Processing and applications of aerosol-assisted chemical vapor deposition, *Chem. Vap. Depos.* 12 (2006) 583–596, <http://dx.doi.org/10.1002/cvde.200600033>.
- [18] P. Marchand, I.A. Hassan, I.P. Parkin, C.J. Carmalt, Aerosol-assisted delivery of precursors for chemical vapour deposition: expanding the scope of CVD for materials fabrication, *Dalton Trans.* 42 (2013) 9406, <http://dx.doi.org/10.1039/c3dt50607j>.
- [19] C.E. Knapp, C.J. Carmalt, Solution based CVD of main group materials, *Chem. Soc. Rev.* 45 (2016) 1036–1064, <http://dx.doi.org/10.1039/C5CS00651A>.
- [20] P. Marchand, C.J. Carmalt, Molecular precursor approach to metal oxide and pnictide thin films, *Coord. Chem. Rev.* 257 (2013) 3202–3221, <http://dx.doi.org/10.1016/j.ccr.2013.01.030>.
- [21] K. Choy, Chemical vapour deposition of coatings, *Prog. Mater. Sci.* 48 (2003) 57–170, [http://dx.doi.org/10.1016/S0079-6425\(01\)00009-3](http://dx.doi.org/10.1016/S0079-6425(01)00009-3).
- [22] D.S. Bhachu, G. Sankar, I.P. Parkin, Aerosol assisted chemical vapor deposition of transparent conductive zinc oxide films, *Chem. Mater.* 24 (2012) 4704–4710, <http://dx.doi.org/10.1021/cm302913b>.
- [23] H. Liang, R.G. Gordon, Atmospheric pressure chemical vapor deposition of transparent conducting films of fluorine doped zinc oxide and their application to amorphous silicon solar cells, *J. Mater. Sci.* 42 (2007) 6388–6399, <http://dx.doi.org/10.1007/s10853-006-1255-5>.
- [24] J. Auld, D.J. Houlton, A.C. Jones, S.A. Rushworth, M.A. Malik, P. O'Brien, G.W. Critchlow, Growth of ZnO by MOCVD using alkylzinc alkoxides as single-source precursors, *J. Mater. Chem.* 4 (1994) 1249, <http://dx.doi.org/10.1039/jm9940401249>.
- [25] J.A. Manzi, C.E. Knapp, I.P. Parkin, C.J. Carmalt, Aerosol-assisted chemical-vapour deposition of zinc oxide from single-source β -iminoesterate precursors: aerosol-assisted chemical vapour deposition of zinc oxide, *Eur. J. Inorg. Chem.* 2015 (2015) 3658–3665, <http://dx.doi.org/10.1002/ajic.201500416>.
- [26] T. Maruyama, J. Shionoya, Zinc oxide thin films prepared by chemical vapour deposition from zinc acetate, *J. Mater. Sci. Lett.* 11 (1992) 170–172, <http://dx.doi.org/10.1007/BF00724682>.
- [27] H. Sato, T. Minami, T. Miyata, S. Takata, M. Ishii, Transparent conducting ZnO thin films prepared on low temperature substrates by chemical vapour deposition using Zn(CSH7O2)2, *Thin Solid Films* 246 (1994) 65–70, [http://dx.doi.org/10.1016/0040-6090\(94\)90733-1](http://dx.doi.org/10.1016/0040-6090(94)90733-1).
- [28] D. Bekermann, A. Ludwig, T. Toader, C. Maccato, D. Barreca, A. Gasparotto, C. Bock, A.D. Wieck, U. Kunze, E. Tondello, R.A. Fischer, A. Devi, MOCVD of ZnO films from bis(ketoimino)Zn(II) precursors: structure, morphology and optical properties, *Chem. Vap. Depos.* 17 (2011) 155–161, <http://dx.doi.org/10.1002/cvde.201006898>.
- [29] M. Vijji, R. Nagarajan, Zinc triflate catalyzed regioselective synthesis of pyrrolo[2,3-c]carbazoles via heteroannulation, *RSC Adv.* 2 (2012) 10544, <http://dx.doi.org/10.1039/c2ra21735j>.
- [30] S. Murarka, A. Studer, Zinc triflate catalyzed aerobic cross-dehydrogenative coupling (CDC) of alkynes with nitrones: a new entry to isoxazoles, *Org. Lett.* 13 (2011) 2746–2749, <http://dx.doi.org/10.1021/ol200849k>.
- [31] D.M. Granum, P.J. Riedel, J.A. Crawford, T.K. Mahle, C.M. Wyss, A.K. Begej, N. Arulsamy, B.S. Pierce, M.P. Mehn, Synthesis and characterization of sterically encumbered β -ketoimino complexes of iron(II) and zinc(II), *Dalton Trans.* 40 (2011) 5881, <http://dx.doi.org/10.1039/c1dt10024f>.
- [32] C.E. Knapp, G. Hyett, I.P. Parkin, C.J. Carmalt, Aerosol-assisted chemical vapor deposition of transparent conductive gallium–indium–oxide films, *Chem. Mater.* 23 (2011) 1719–1726, <http://dx.doi.org/10.1021/cm102292b>.
- [33] R.K. Shukla, A. Srivastava, A. Srivastava, K.C. Dubey, Growth of transparent conducting nanocrystalline Al doped ZnO thin films by pulsed laser deposition, *J. Cryst. Growth* 294 (2006) 427–431, <http://dx.doi.org/10.1016/j.jcrysgro.2006.06.035>.
- [34] B.S. Shaheen, H.G. Salem, M.A. El-Sayed, N.K. Allam, Thermal/electrochemical growth and characterization of one-dimensional ZnO/TiO₂ hybrid nanoelectrodes for solar fuel production, *J. Phys. Chem. C* 117 (2013) 18502–18509, <http://dx.doi.org/10.1021/jp405515v>.
- [35] S. Kaleemulla, N. Madhusudhana Rao, M. Girish Joshi, A. Sivasankar Reddy, S. Uthanna, P. Sreedhara Reddy, Electrical and optical properties of In₂O₃:Mo thin films prepared at various Mo-doping levels, *J. Alloys Compd.* 504 (2010) 351–356, <http://dx.doi.org/10.1016/j.jallcom.2010.05.068>.
- [36] J. Tauc, Optical properties and electronic structure of amorphous Ge and Si, *Mater. Res. Bull.* 3 (1968) 37–46, [http://dx.doi.org/10.1016/0025-5408\(68\)90023-8](http://dx.doi.org/10.1016/0025-5408(68)90023-8).
- [37] V. Srikant, D.R. Clarke, On the optical band gap of zinc oxide, *J. Appl. Phys.* 83 (1998) 5447, <http://dx.doi.org/10.1063/1.367375>.
- [38] S.T. Tan, B.J. Chen, X.W. Sun, W.J. Fan, H.S. Kwok, X.H. Zhang, S.J. Chua, Blueshift of optical band gap in ZnO thin films grown by metal–organic chemical-vapor deposition, *J. Appl. Phys.* 98 (2005) 13505, <http://dx.doi.org/10.1063/1.1940137>.
- [39] M. Purica, Optical and structural investigation of ZnO thin films prepared by chemical vapor deposition (CVD), *Thin Solid Films* 403–404 (2002) 485–488, [http://dx.doi.org/10.1016/S0040-6090\(01\)01544-9](http://dx.doi.org/10.1016/S0040-6090(01)01544-9).
- [40] E. Burstein, Anomalous optical absorption limit in InSb, *Phys. Rev.* 93 (1954) 632–633, <http://dx.doi.org/10.1103/PhysRev.93.632>.
- [41] T.S. Moss, The interpretation of the properties of indium antimonide, *Proc. Phys. Soc. Sec. B* 67 (1954) 775.
- [42] X.-J. Qin, S.-H.-Z. Han, L. Zhao, H.-T. Zuo, S.-T. Song, Fabrication of transparent conductive Al-doped ZnO thin films by aerosol-assisted chemical vapour deposition: fabrication of transparent conductive Al-doped ZnO thin films by aerosol-assisted chemical vapour deposition, *J. Inorg. Mater.* 26 (2011) 607–612, <http://dx.doi.org/10.3724/SP.J.1077.2011.00607>.
- [43] N. Hirahara, B. Onwona-Agyeman, M. Nakao, Preparation of Al-doped ZnO thin films as transparent conductive substrate in dye-sensitized solar cell, *Thin Solid Films* 520 (2012) 2123–2127, <http://dx.doi.org/10.1016/j.tsf.2011.08.100>.